





# Implications of an Extended Dark Energy Model with Massive Neutrinos

Ravi Kumar Sharma, Kanhaiya Lal Pandey , and Subinoy Das Indian Institute of Astrophysics, Bengaluru, Karnataka 560034, India; [ravi.sharma@iiap.res.in](mailto:ravi.sharma@iiap.res.in), [kanhaiya.pandey@iiap.res.in](mailto:kanhaiya.pandey@iiap.res.in), [subinoy@iiap.res.in](mailto:subinoy@iiap.res.in)

Received 2022 April 20; revised 2022 June 14; accepted 2022 June 16; published 2022 July 29

## Abstract

Recently there have been reports of finding a lower bound on the neutrino mass parameter ( $\Sigma m_\nu$ ) when using the Atacama Cosmology Telescope (ACT) and SPTpol data; however, these bounds on the  $\Sigma m_\nu$  are still weaker for most cases around the  $1\sigma$  level. In this context, here in this work, we study the consequences of using an enlarged four parameter dynamical dark energy equation of state on the neutrino mass parameter as well as on the Hubble and S8 tensions. The four parameter dark energy equation of state incorporates a generic nonlinear monotonic evolution of the dark energy equation of state, where the four parameters are the early and the present value of the equation of state, the transition scale factor, and the sharpness of the transition. We report that with lensing-marginalized Planck + BAO + Pantheon and prior on absolute magnitude  $M_B$ , and KIDS/Viking  $S_8$  prior, the model favors a nonzero value for the neutrino mass parameter at most at the  $1\sigma$  level ( $\Sigma m_\nu = 0.1847^{+0.0698}_{-0.165}$  eV). In this case this model also brings down the Hubble tension to a  $2.5\sigma$  level and the S8 tension to a  $\sim 1.5\sigma$  level. This model also provides tighter constraints on the value of the dark energy equation of state at present epoch  $w_0$  ( $w_0 = -0.9901^{+0.0561}_{-0.0766}$ ) in comparison to the Chevalier-Polarski and Linder-like parameterization.

*Unified Astronomy Thesaurus concepts:* [Dark energy \(351\)](#)

## 1. Introduction

The observations of Type Ia supernovae (SNe) show that the expansion of the universe is accelerating. The acceleration requires the universe to be dominated by an exotic fluid with negative pressure. The simplest explanation for dark energy (DE) is the cosmological constant or vacuum energy that explains the acceleration of the universe. The cosmological constant is preferred from cosmological observations yet its theoretical understanding has been questionable (Sahni 2002). The other alternatives of the cosmological constant that can act as dark energy are scalar fields such as the quintessence field, modified gravity, and phantom dark energy (Ballardini et al. 2016; Nojiri et al. 2017; Braglia et al. 2021; Farhang & Khosravi 2021). There has not been any observational evidence of such alternatives but it has not been ruled out either. One such model is dynamical dark energy driven by a slowly rolling scalar field. If this is true, then it opens up many new observational windows that may shed light on the fundamental nature of this mysterious component of the universe.

The other reason to explore beyond the  $\Lambda$ CDM model is the recently emerging and persistent anomalies in present high precision cosmological data. The mismatch between values of the Hubble parameter inferred from cosmic microwave background (CMB) data and direct measurements is one of them. The SH0ES (Supernovae H0 for Equation of State) team has measured the value of the Hubble parameter  $H_0 = 73.2 \pm 1.3 \text{ km s}^{-1} \text{ Mpc}^{-1}$  using the distance ladder method (Riess et al. 2019, 2021). However the Planck 2018 measurement of the CMB has measured the value of the Hubble parameter  $H_0 = 67.36 \pm 0.54 \text{ km s}^{-1} \text{ Mpc}^{-1}$  using the  $\Lambda$ CDM model (Planck Collaboration et al. 2020), so there is a  $4.2\sigma$  discrepancy between both measurements. This mismatch gained significance

with various improved precision measurements; see, Freedman (2017), Schöneberg et al. (2021), Di Valentino (2021), and Di Valentino et al. (2021a, 2021b).

Similarly there is another tension related to the measured value of  $S_8 \equiv \sigma_8 (\Omega_m/0.3)^{0.5}$ , where  $\sigma_8$  is the rms of matter fluctuations on a  $8 h^{-1} \text{ Mpc}$  scale, and  $\Omega_m$  is the total matter abundance. The latest prediction from Planck CMB data within the  $\Lambda$ CDM framework is  $S_8 = 0.832 \pm 0.013$  (Planck Collaboration et al. 2020).

Originally, observations of galaxies through weak lensing by the CFHTLenS Collaboration have indicated that the  $\Lambda$ CDM model predicts a  $S_8$  value that is larger than the direct measurement at the  $2\sigma$  level (Heymans et al. 2013; MacCrann et al. 2015). This tension has since then been further established within the KiDS/Viking data (Hildebrandt et al. 2020; Joudaki et al. 2020), but is milder within the Dark Energy Survey (DES) data (Abbott et al. 2018). However, a reanalysis of the DES data, combined with KiDS/Viking, leads to a determination of  $S_8$  that is discrepant with Planck at the  $3\sigma$  level;  $S_8 = 0.755^{+0.019}_{-0.021}$  (Joudaki et al. 2020). Recently, the combination of KiDS/Viking and Sloan Digital Sky Survey (SDSS) data has established  $S_8 = 0.766^{+0.02}_{-0.014}$  (Heymans et al. 2021). However, a study in Nunes & Vagnozzi (2021) shows fainter  $S_8$  tension when redshift-space distortions data are included.

There has been a wide range of solutions proposed to solve these cosmological tensions, which require new physics/modifications in the early universe, i.e., prerecombination era as well as in the late universe. Not a single model yet fully solves both  $H_0$  and  $S_8$  tensions simultaneously. The class of solutions that invokes modifications of the late-time universe dynamics in dark energy generally leaves  $r_s$  unaffected by construction and has been studied extensively in recent times. The higher value of  $H_0$  is then accommodated by a smaller value of  $\Omega_{\text{DE}}$  or  $\Omega_m$  at redshift below  $z_*$  such that  $d_A(z_*)$  stays unaffected as well. This can be done for instance by invoking variations in the dark energy equation of state (Di Valentino et al. 2015, 2016b, 2017; Poulin et al. 2019; Bhattacharyya et al. 2019; Visinelli et al. 2019; Vagnozzi 2020; Gogoi et al. 2021; Hazra et al. 2022), or

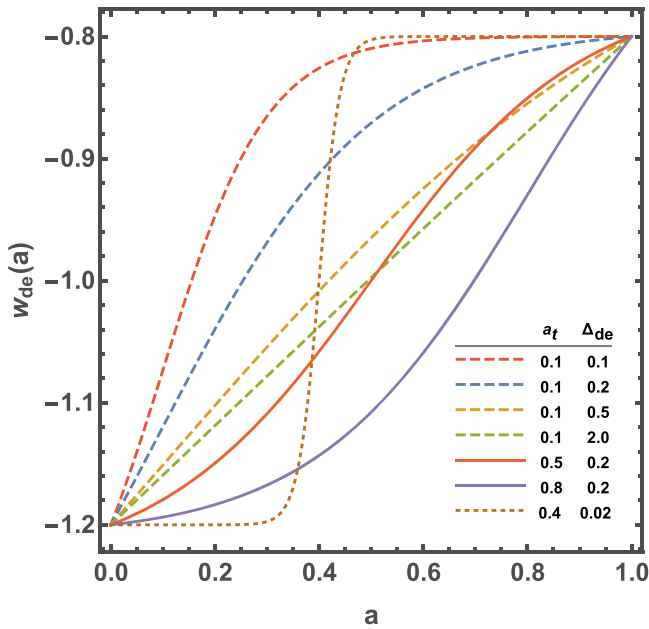


**Figure 1.** Evolution of  $w_{de}$  for different sets of values for  $a_t$  and  $\Delta_{de}$ , parameters  $w_0$  and  $w_m$  are fixed to  $-0.8$  and  $-1.2$ , respectively.

decaying dark matter (Poulin et al. 2016; Pandey et al. 2020; Abellán et al. 2021b), or nonthermal dark matter (Das et al. 2022) with a certain level of success.

The study of the dynamical behavior of dark energy is often done in terms of its equation of state  $w(z) = \frac{P(z)}{\rho(z)}$  that can vary as a function of redshift. Equation of state  $w = -1$  corresponds to the cosmological constant. There are some recent studies where it has been shown that the solving of  $H_0$  and  $S_8$  tensions requires  $w(z) < -1$  at some  $z > 0$  and time-varying dark energy equations of state, which cross the phantom barrier (Heisenberg et al. 2022a). Also it has been shown that a large class of quintessence ( $w > -1$ ) models including the ones that arise from string swampland conjecture lower the  $H_0$  parameter and thereby make the  $H_0$  tension worse (Banerjee et al. 2021); however, interacting DE models, for example, Das et al. (2006), where the variation in  $w(z)$  starts from a higher redshift might indeed alleviate the  $H_0$  anomaly. From observations, it is required that equations of state at present time should be consistent with value  $w \approx -1$ ; however, constraints on the equation of state at higher redshift are weaker. There have already been several efforts to parameterize the equation of state of dark energy. Some recent works in this direction can be found in Efstathiou (1999), Chevallier & Polarski (2001), Linder (2003), Jassal et al. (2005), Barboza & Alcaniz (2008), Bamba et al. (2012), Marcondes & Pan (2017), Durrive et al. (2018), Jaber & de la Macorra (2018), Martins & Colomer (2018), Li & Shafieloo (2019), Anchordoqui et al. (2021), Colgáin et al. (2021), Mawas et al. (2021), Theodoropoulos & Perivolaropoulos (2021), Yang et al. (2021a), Yang et al. (2021b), Heisenberg et al. (2022b), and Roy et al. (2022).

We explore in detail the possibility of dynamical DE with a more general model-independent approach where we go beyond the Chevallier-Polarski and Linder (CPL) parameterization (Chevallier & Polarski 2001; Linder 2003) where the dark energy equation of state  $w$  evolves linearly with expansion factor  $a$ . To be specific, in this paper, we study a generic nonlinearly evolving equation of state. Some of the recent works on the dynamical dark energy scenario such as Colgáin et al. (2021) suggest that CPL

parameterization is not sensitive at low redshifts and thus provides motivation for going beyond CPL-like parameterization. It was recently pointed out that if late-time cosmology is modified through time-varying  $w$ , one indeed should use the direct prior on the absolute magnitude of supernovae,  $M_B$  instead of  $H_0$  prior (Lemos et al. 2019; Benevento et al. 2020; Camarena & Marra 2021; Efstathiou 2021). To our knowledge, this work is the first work where we present a detailed analysis of a four parameter dynamical dark energy model. To do so, we use a generic four parameter model of dynamical dark energy equation of state  $w$  originally proposed in Corasaniti & Copeland (2003) and test it against the recent Planck 2018, Pantheon, and baryon acoustic oscillations (BAO) data sets. In comparison to CPL parameterization, this parameterization has two extra parameters to incorporate the possible nonlinear evolution of the equation of state with time. The main interest of this parameterization is that it captures possible transition in the equation of state of the dynamical dark energy during the course of its evolution, which many quintessence/K-essence and phantom dark energy models exhibit (Corasaniti & Copeland 2003).

Earlier studies have shown that the total neutrino mass parameter  $\Sigma m_\nu$  shows a significant amount of degeneracy with other cosmological parameters (e.g., with the matter density parameter  $\Omega_m$  and the Hubble parameter  $H_0$ ) if we just use the CMB data alone. Moreover for models with a variable  $w(z)$ , the constraint from CMB is essentially on one number that is the effective equation of state  $w_{eff}$  (Jassal et al. 2010). Adding low redshift measurement data such as the BAO and the SNE data can help in breaking these degeneracies (Di Valentino et al. 2016a; Sutherland 2018) and thus in getting better constraints on the  $\Sigma m_\nu$  and the DE parameters.

In this study, we find that all four parameters of the equation of state cannot be constrained fully with current observational data. Especially, Planck 2018 data alone have a poor constraining ability on dark energy parameters. Once we include the BAO and Pantheon data, the constraints improve and the Hubble tension comes down to a  $2.5\sigma$  level from the SH0ES measurement, and the  $S_8$  tension comes down to  $1.5\sigma$  from the KIDS/Viking measurement.

An important aspect of this paper is to get neutrino mass constraints in the 4pDE model. Standard massive neutrinos play an important role in the evolution of the universe; they leave a nonnegligible impact on the CMB and large-scale structure at different epochs of the evolution of the universe. This impact is used to get a bound on neutrino mass. Some of the effects of standard model neutrinos and dark energy are the same during specific cosmic time. Therefore the nature of dark energy has an important role in constraining neutrino mass. Some of the relevant studies we find in the literature are Hannestad (2005), Calabrese et al. (2011), Lorenz et al. (2017), Vagnozzi et al. (2017), Poulin et al. (2018), Vagnozzi et al. (2018), Abellán et al. (2021a), and Di Valentino & Melchiorri (2022). In our analysis, we detect a nonzero neutrino mass at  $1\sigma$  level ( $\Sigma m_\nu \sim 0.2 \pm 0.1$  eV) but consistent with zero at  $2\sigma$  level unlike a previous study (Poulin et al. 2018) where the analysis was done with earlier (2015) Planck data and the neutrino mass  $\Sigma m_\nu$  was found to be nonzero even at  $\gtrsim 2\sigma$ .

The plan of the paper is as follows. A brief description of the four parameter dynamical dark energy equation of state,  $w_{de}(a)$ , is given in Section 2. In Sections 3 and 4 we provide a detailed description of our analysis and results. Then Section 5 summarizes the paper and future outlook.

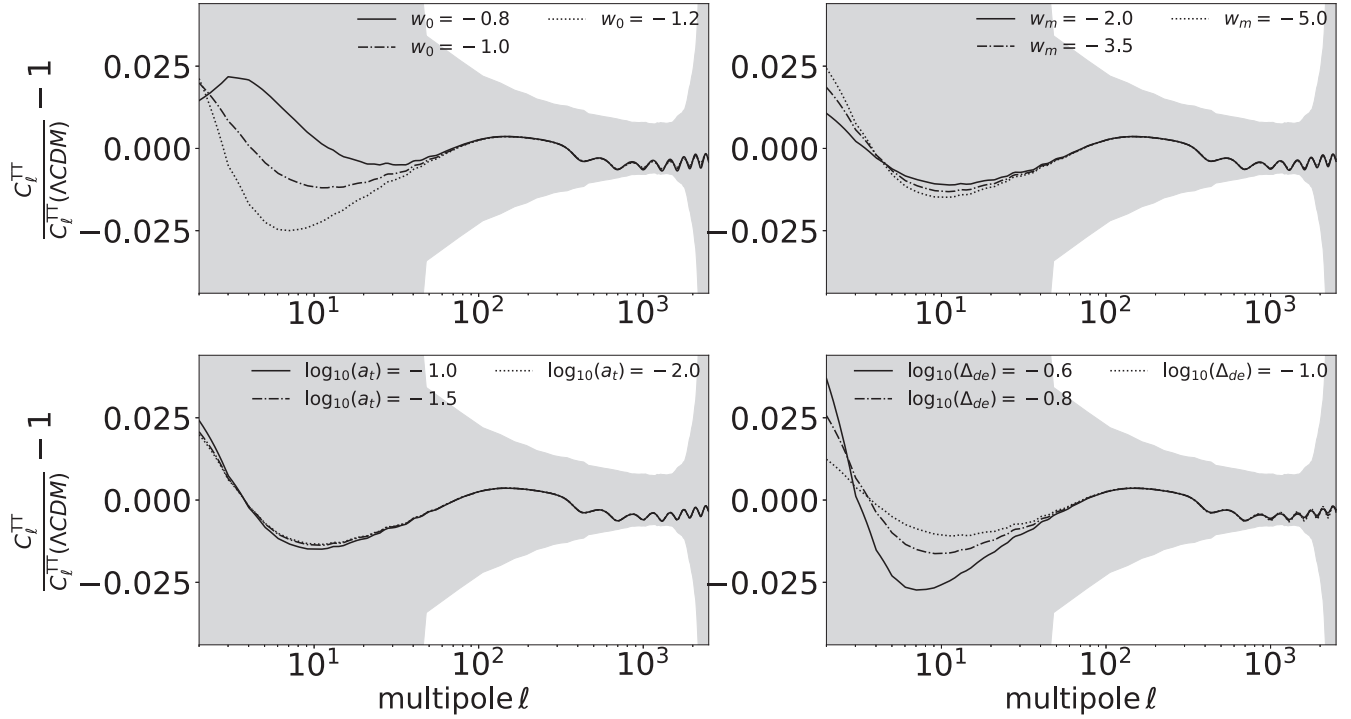


**Figure 2.** The residual plots of CMB TT power spectra for the 4pDE model with respect to the  $\Lambda$ CDM model. The shaded region is the Planck 2018  $1\sigma$  uncertainties. Each of the four panels show effects of varying different dark energy equation of state (EOS) parameters (see the legends) while fixing other EOS parameters to values ( $w_0 = -1.03$ ,  $w_m = -3.97$ ,  $\log_{10}(a_t) = -1.63$ ,  $\log_{10}(\Delta_{de}) = -0.87$ ).

## 2. Four Parameter Model for Dark Energy

To investigate the effect of a nonlinearly evolving dark energy equation of state, we use a model-independent, four parameter dynamical dark energy equation of state  $w_{de}(a)$ , suggested by Corasaniti & Copeland (2003),

$$w_{de}(a) = w_0 + (w_m - w_0) \times \Gamma(a), \quad (1)$$

where  $w_0$  and  $w_m$  are two parameters denoting the initial and final values of the dark energy equation of state, i.e.,  $w_0 = w_{de}(a=1)$  and  $w_m = w_{de}(a \ll 1)$ . The factor  $\Gamma(a)$  contains the other two parameters describing the course of the evolution of  $w_{de}(a)$ , and is given as,

$$\Gamma(a) = \frac{1 - \exp(-(a-1)/\Delta_{de})}{1 - \exp(1/\Delta_{de})} \times \frac{1 + \exp(a_t/\Delta_{de})}{1 + \exp(-(a-a_t)/\Delta_{de})}, \quad (2)$$

where  $a_t$  is the scale factor at which the transition from  $w_m$  to  $w_0$  takes place and the  $\Delta_{de}$  is the steepness of the transition.

The factor  $\Gamma(a)$  in Equation (1), characterizes the course of the evolution of  $w_{de}(a)$ . Figure 1 elaborates the nature of the parameters  $a_t$  and  $\Delta_{de}$ . It can be easily shown that for the two extreme limits of  $\Delta_{de}$  Equation (1) takes the following form,

$$\lim_{\Delta_{de} \rightarrow \infty} w_{de}(a) = w_0 + (w_m - w_0) \times (1 - a) \quad (3)$$

$$\lim_{\Delta_{de} \rightarrow 0} w_{de}(a) = w_0 + \Theta(a_t - a) \times (w_m - w_0), \quad (4)$$

i.e., Equation (1) approaches standard two parameter parameterization with  $w_a = w_m - w_0$  in the limit of  $\Delta_{de} \rightarrow \infty$  as this is also evident from the green-dashed plot in the Figure 1. Also when  $\Delta_{de} \rightarrow 0$  the function  $\Gamma(a)$  tends to become a step

**Table 1**  
List of Parameter Priors for the Additional Parameters

Parameter	Prior
$w_0$	$[-5, -0.5]$
$w_m$	$[-5, -0.5]$
$\log(a_{de})$	$[-3, 0]$
$\log(\Delta_{de})$	$[-1, 0]$
$\Sigma m_\nu$	$[0, 5]$

**Note.** Priors for the standard base parameters  $\{\omega_b, \omega_{cdm}, 100 \times \theta_s, n_s, \ln(10^{10} A_s), \tau_{reio}\}$  are kept the same as the default set into the MontePython-v3 (Brinckmann 2019) code.

**Table 2**  
Best-fit  $\chi^2$  per Experiment (and Total) in the  $\nu$ 4pDE Model

Data Set ↓	$\nu$ 4pDE			
	I	II	III	IV
Planck high $-\ell$ TT, TE, EE	2345.70	2347.49	2347.84	2349.06
Planck low $-\ell$ EE	396.31	395.78	396.16	396.90
Planck low $-\ell$ TT	23.56	22.87	22.86	22.76
Planck lensing	8.84	8.95	8.70	9.37
Pantheon	1026.90	1027.22	1027.89	1027.93
BAO FS BOSS DR12	7.15	7.18	8.52	9.96
BAO BOSS low $-z$	1.63	2.68	3.245	3.47
Absolute M	...	13.05	10.43	...
SHOES	...	...	...	9.865
S8	...	...	4.717	2.15
Total	3810.13	3825.18	3830.39	3831.50

**Note.** The column headings in Roman numerals correspond to different data/prior combinations as (I) Planck+Ext; (II) Planck+Ext+MB; (III) Planck+Ext+MB+S8; (IV) Planck+Ext+H0+S8.

**Table 3**The Mean (Best-fit)  $\pm 1\sigma$  Error of the Cosmological Parameters Reconstructed from the Lensing-marginalized Planck+BAO+SN1a Data and Combinations of  $M_B$  and  $S_8$  Priors for the  $\nu\Lambda$ pDE Model

Parameter	$\nu\Lambda$ pDE			
	Planck+Ext	Planck+Ext+ $M_B$	Planck+Ext+ $M_B$ + $S_8$	Planck+Ext+ $H_0$ + $S_8$
100 $\omega_b$	2.231(2.235) $^{+0.01423}_{-0.01359}$	2.235(2.247) $^{+0.01554}_{-0.01479}$	2.239(2.249) $^{0.0155}_{-0.0148}$	2.238(2.239) $^{+0.015}_{-0.015}$
$\omega_{\text{cdm}}$	0.1202(0.1202) $^{+0.00108}_{-0.0010613}$	0.1200(0.1185) $^{+0.0010481}_{-0.0010872}$	0.1193(0.1191) $^{0.00105}_{-0.00109}$	0.1194(0.1192) $^{+0.0011}_{-0.001}$
100 $^*\theta_s$	1.0418(1.0417) $^{+0.00028}_{-0.0003067}$	1.0419(1.0419) $^{+0.0003093}_{-0.0002753}$	1.0419(1.0419) $^{0.000309}_{-0.000273}$	1.042(1.04198) $^{+0.00029}_{-0.00028}$
$n_s$	0.9631(0.9642) $^{0.0038948}_{-0.004134}$	0.9636(0.9679) $^{0.004000}_{-0.0042631}$	0.9647(0.9652) $^{0.004}_{-0.00426}$	0.9645(0.9644) $^{+0.0042}_{-0.0042}$
$\ln(10^{10}A_s)$	3.043(3.047) $^{+0.0150}_{-0.0147}$	3.042(3.037) $^{+0.01488}_{-0.014812}$	3.042(3.040) $^{0.0149}_{-0.0148}$	3.042(3.0469) $^{+0.015}_{-0.016}$
$\tau_{\text{reio}}$	0.0537(0.0555) $^{+0.007626}_{-0.007351}$	0.05357(0.05308) $^{+0.0072268}_{-0.007737}$	0.05436(0.05511) $^{+0.00723}_{-0.00754}$	0.054(0.0577) $^{+0.0076}_{-0.0079}$
$\Sigma m_\nu$ [eV]	0.1129(0.038) $^{0.0276}_{-0.1129}$	0.1069(0.0094) $^{0.0697}_{-0.1069}$	0.1847(0.1043) $^{0.0698}_{-0.165}$	0.1857(0.2748) $^{+0.091}_{-0.13}$
$w_0$	-0.9856(-1.038) $^{+0.053}_{-0.065}$	-0.9886(-1.011) $^{+0.053}_{-0.073}$	-0.9901(-1.029) $^{0.0561}_{-0.0766}$	-1.04(-0.9446) $^{+0.049}_{-0.062}$
$w_m$	-2.285(-1.040) $^{+1.5}_{-0.59}$	-2.715(-1.611) $^{+1.6}_{-0.91}$	unconstrained	-2.45(-3.1) $^{+1.4}_{-0.78}$
$\log_{10}(a_i)$	unconstrained	unconstrained	unconstrained	unconstrained
$\log_{10}(\Delta_{\text{de}})$	-0.6752(-0.7649) $^{+0.066}_{-0.32}$	-0.6687(-0.9264) $^{+0.065}_{-0.35}$	-0.6313(-0.8739) $^{0.0809}_{-0.368}$	-0.6936(-0.4452) $^{+0.068}_{-0.31}$
$M_B$	-19.40(-19.40) $^{+0.01887}_{-0.01862}$	-19.37(-19.37) $^{+0.01629}_{-0.01655}$	-19.369(-19.359) $^{+0.01580}_{-0.01615}$	-19.37(-19.36) $^{+0.017}_{-0.015}$
$\sigma_8$	0.8135(0.8279) $^{+0.01685}_{-0.01203}$	0.8225(0.8216) $^{+0.01658}_{-0.01303}$	0.8073(0.8206) $^{+0.01763}_{-0.01462}$	0.8093(0.7966) $^{+0.017}_{-0.014}$
$\Omega_m$	0.3064(0.3038) $^{+0.00779}_{-0.00810}$	0.2973(0.2954) $^{+0.0069}_{-0.0074}$	0.294(0.2893) $^{0.00637}_{-0.00654}$	0.2919(0.2955) $^{+0.006}_{-0.0064}$
$S_8$	0.822(0.832) $^{+0.0170}_{-0.0117}$	0.8188(0.81) $^{+0.016}_{-0.013}$	0.799(0.8051) $^{0.0163}_{-0.0134}$	0.7982(0.8043) $^{+0.014}_{-0.013}$
$H_0$ [kms $^{-1}$ Mpc $^{-1}$ ]	68.21(68.53) $^{+0.846}_{-0.823}$	69.22(69.14) $^{+0.843}_{-0.791}$	69.44(69.87) $^{0.697}_{-0.724}$	69.71(69.58) $^{+0.7}_{-0.7}$
$\chi^2_{\text{min}}$	3810.13	3825.18	3830.34	3831.50
$\Delta\chi^2_{\text{min}}$	-1.4	-6.53	-5.5	-4.3

**Note.** We also report the corresponding  $\Delta\chi^2_{\text{min}}$  values.

function (Heaviside function,  $\Theta$ ) around  $a = a_t$  (the orange-dotted plot in Figure 1).

Our parameterization is generic to a class of noninteracting scalar field dynamical dark energy models only, i.e., we assume  $c_{s,\text{de}}^{\text{eff}} = 1$ . Also this parameterization can only mimic monotonically evolving dynamical dark energy models.

We will consider a homogeneous and isotropic flat background for the universe described by a FLRW metric. If we neglect the radiation density today, the Friedmann equation will have the following form,

$$\frac{H^2}{H_0^2} = \Omega_M/a^3 + \Omega_{\text{DE}} \exp\left(3 \times \int_1^a \frac{1 + w_{\text{de}}(a')}{a'} da'\right), \quad (5)$$

where  $\Omega_M$  and  $\Omega_{\text{DE}}$  are matter density and dark energy density parameters, respectively, and for a flat universe  $\Omega_{\text{DE}} + \Omega_M = 1$ .

## 2.1. Effect on Various Cosmological Observables

### 2.1.1. Effect on CMB

Though the dark energy energy starts to dominate the energy content of the universe at late times, still it can affect the CMB data in two ways: one is by affecting the angular diameter distance and the second is through the Integrated Sachs–Wolfe (ISW) effect. The change in the angular diameter distance is reflected in shifts in the location of the peaks in CMB angular power spectra. On the other hand the late-time ISW is sensitive to the low  $\ell$  regime of the CMB angular power spectra. Figure 2 shows the effect of the individual dark energy parameters ( $w_0$ ,  $w_m$ ,  $a_t$ ,  $\Delta_{\text{de}}$ ) on the CMB temperature angular power spectrum while keeping the other parameters fixed.

### 2.1.2. Effect on BAO

We know the BAO scale can act as a standard ruler. This scale can be used to measure the angular diameter distance,  $d_A(z) = c/(1+z) \int_0^z 1/H(z') dz'$ , using clustering of galaxies perpendicular to the line of sight and expansion rate  $H(z)$  of the universe using clustering along the line of sight. Adjustments in cosmological parameters can alter the clustering scale of the galaxies, which is related to the sound horizon  $r_d = \int_{z_d}^{\infty} c_s(z)/H(z) dz$ , where  $c_s$  is the sound speed and  $z_d$  is the drag epoch. Effectively, BAO measurements actually constrain the combination  $r_d^* H(z)$  or  $d_A(z)/r_d$ . Another important observable in redshift surveys is  $f\sigma_8$ , which is defined as a combination of growth rate  $f(a)$  and the rms normalization of the matter power spectrum  $\sigma_8$ ,

$$f\sigma_8(a) = a \frac{\delta'_m(a)}{\delta_m(1)} \sigma_{8,0}.$$

Figures 7 and 8 in the Appendix, respectively, show the effect of the individual dark energy parameters ( $w_0$ ,  $w_m$ ,  $a_t$ ,  $\Delta_{\text{de}}$ ) on the quantities  $r_d \times H(z)/(1+z)$  and  $f(z) \times \sigma_8(z)$  while keeping the other parameters fixed.

### 2.1.3. Supernovae Ia Data

SNe data provide geometric constraints for dark energy evolution. These constraints are obtained by comparing the predicted luminosity distance to the SNe with the observed ones. The theoretical model and observations are compared with the measured luminosities,

$$M = m - 5 \log_{10}\left(\frac{d_L}{10}\right),$$

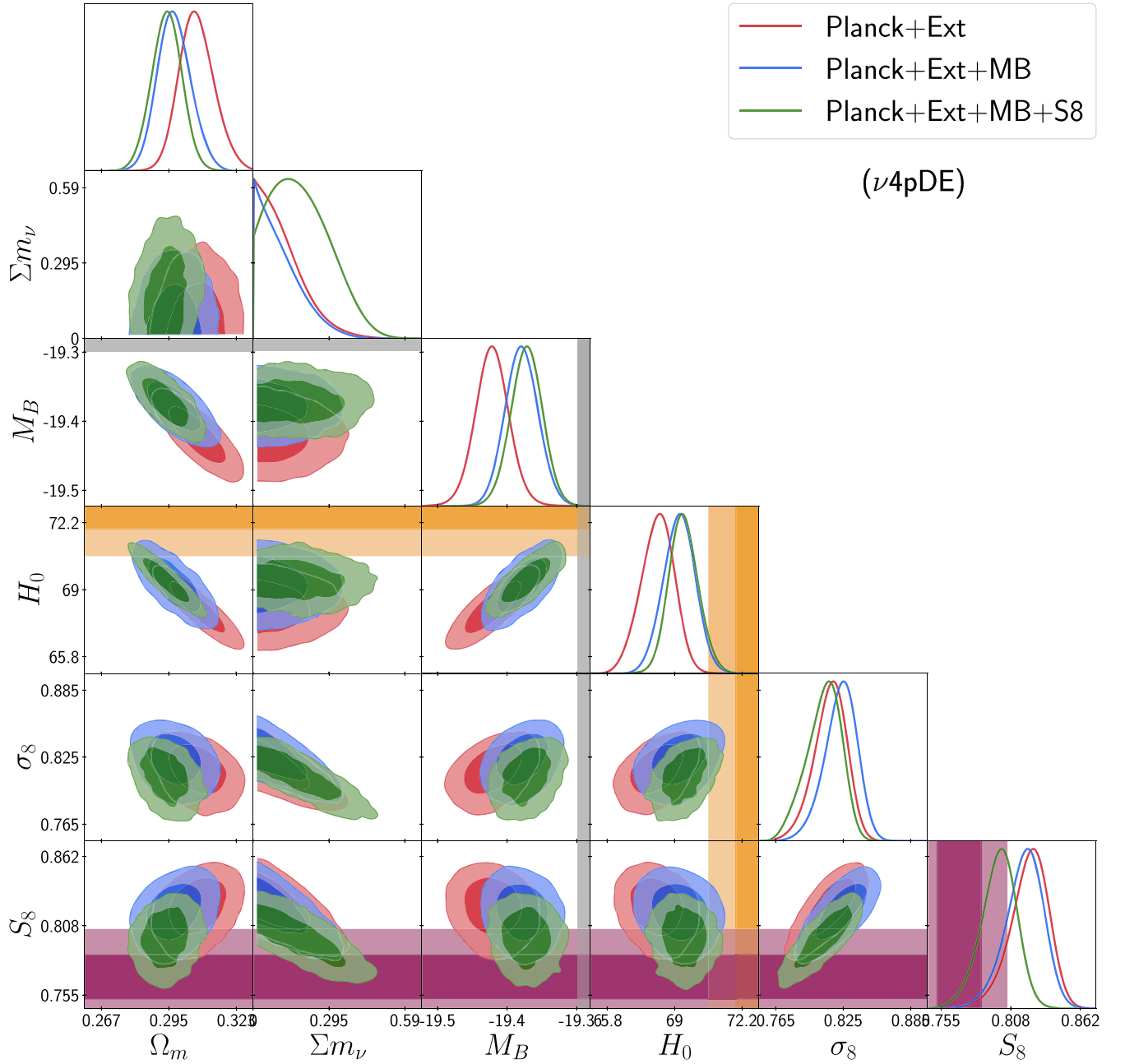


**Figure 3.** 2D posterior distributions of ( $\Omega_m$ ,  $\Sigma m_\nu$ ,  $M_B$ ,  $H_0$ ,  $\sigma_8$ ,  $S_8$ ) for the  $\nu 4pDE$  model with Planck+Ext data and a different prior combination. We have also added 68% (dark orange) and 95% (light orange) bands corresponding to a  $H_0$  measurement from SH0ES and 68% (dark purple) and 95% (light purple) bands corresponding to an  $S_8$  measurement from KIDS1000+BOSS+2dfLenS.

where  $M$  is absolute magnitude of the SNe,  $m$  is apparent magnitude of the SNe, and  $d_L = c (1 + z) \int_0^z 1/H(z') dz'$  is their luminosity distance in parsec. This depends on the evolution of dark energy through  $H(z)$ . Figure 9 in the Appendix shows the effect of the individual dark energy parameters ( $w_0$ ,  $w_m$ ,  $a_1$ ,  $\Delta_{de}$ ) on  $d_L(z)$  while keeping the other parameters fixed.

### 3. Details of Analysis

#### 3.1. Data Sets

1. Planck 2018 measurements of the low- $\ell$  CMB temperature auto correlation (TT), E-mode polarization auto correlation (EE), and high- $\ell$  TT, temperature E-mode cross-correlation (TE), EE power spectra, together with the gravitational lensing potential reconstruction (Planck Collaboration et al. 2020).
2. The BAO measurements from 6dFGS at  $z=0.106$  (Beutler et al. 2011), SDSS DR7 at  $z=0.15$  (Ross et al. 2015), BOSS DR12 at  $z=0.38, 0.51, \text{ and } 0.61$  (Alam et al. 2017), and the joint constraints from eBOSS DR14 Ly $\alpha$  autocorrelation at  $z=2.34$  (de Sainte Agathe et al. 2019), and cross correlation at  $z=2.35$  (Blomqvist et al. 2019).
3. The measurements of the growth function  $f\sigma_8(z)$  (FS) from the CMASS and LOWZ galaxy samples of BOSS DR12 at  $z=0.38, 0.51, \text{ and } 0.61$  (Alam et al. 2017).

**Table 4**The Mean (Best-fit)  $\pm 1\sigma$  Error of the Cosmological Parameters Reconstructed from the Lensing-marginalized Planck+BAO+SN1a Data and Combinations of  $M_B$  and  $S_8$  Priors for the  $\nu$ CPL Model

Parameter	$\nu$ CPL		
	Planck+Ext	Planck+Ext+ $M_B$	Planck+Ext+ $S_8$ + $M_B$
100 $\omega_b$	2.2334(2.23425) $^{+0.01460}_{-0.01418}$	2.2364(2.2461) $^{+0.01429}_{-0.01442}$	2.239(2.2291) $^{+0.015}_{-0.015}$
$\omega_{\text{cdm}}$	0.12016(0.1197) $^{+0.001131}_{-0.001073}$	0.1201(0.1196) $^{+0.0011}_{-0.0011}$	0.1194(0.1189) $^{+0.0011}_{-0.0011}$
100 $\times\theta_s$	1.0419(1.197716) $^{+0.0002927}_{-0.0003023}$	1.042(1.04173) $^{+0.0003}_{-0.00028}$	1.042(1.0418) $^{+0.00028}_{-0.00031}$
$\ln(10^{10}A_s)$	3.0448(1.197716) $^{+0.01478}_{-0.01570}$	3.043(3.0378) $^{+0.015}_{-0.015}$	3.041(3.0268) $^{+0.015}_{-0.015}$
$n_s$	0.96397(0.9657) $^{+0.00416}_{-0.00394}$	0.9641(0.9657) $^{+0.0041}_{-0.0041}$	0.9645(0.9669) $^{+0.0041}_{-0.0042}$
$\tau_{\text{reio}}$	0.05446(0.05415) $^{+0.00752}_{-0.00801}$	0.05375(0.05149) $^{+0.0074}_{-0.0077}$	0.05388(0.04686) $^{+0.0073}_{-0.0074}$
$\Sigma m_\nu$ [eV]	0.1092(0.04848) $^{+0.0255}_{-0.100}$	0.09942(0.00578) $^{+0.025}_{-0.099}$	0.1877(0.074) $^{+0.094}_{-0.14}$
$w_0$	-0.9690(-0.99195) $^{+0.0787}_{-0.0830}$	-0.9541(-0.9558) $^{+0.076}_{-0.094}$	-0.9393(-1.08) $^{+0.09}_{-0.095}$
$w_a$	-0.2915(-0.1680) $^{+0.409}_{-0.292}$	-0.5008(-0.3023) $^{+0.49}_{-0.28}$	-0.6716(0.0303) $^{+0.55}_{-0.39}$
$M_B$	-19.40(-19.3923) $^{+0.0191}_{-0.0179}$	-19.37(-19.374) $^{+0.016}_{-0.016}$	-19.37(-19.376) $^{+0.016}_{-0.017}$
$\sigma_8$	0.8134(0.8237) $^{+0.0155}_{-0.0120}$	0.8237(-0.8306) $^{+0.016}_{-0.012}$	0.8061(0.8172) $^{+0.018}_{-0.015}$
$\Omega_m$	0.3074(0.3017) $^{+0.00723}_{-0.00808}$	0.2974(0.2977) $^{+0.00664}_{-0.00718}$	0.2948(0.2860) $^{+0.00673}_{-0.00703}$
$S_8$	0.8233(0.827) $^{+0.0156}_{-0.0124}$	0.820(0.825) $^{+0.0152}_{-0.0125}$	0.798(0.802) $^{+0.0157}_{-0.0127}$
$H_0$ [kms $^{-1}$ Mpc $^{-1}$ ]	68.09(68.62) $^{+0.824}_{-0.768}$	69.23(69.10) $^{+0.740}_{-0.742}$	69.36(69.71) $^{+0.720}_{-0.772}$
$\chi^2_{\text{min}}$	3809.86	3824.43	3833.08
$\Delta\chi^2_{\text{min}}$	-1.67	-7.23	-2.76

**Note.** We also report the corresponding  $\Delta\chi^2_{\text{min}}$  values.

- The Pantheon SNIa catalog, spanning redshifts  $0.01 < z < 2.3$  (Scolnic et al. 2018).
- The SH0ES result, modeled with a Gaussian likelihood centered on  $H_0 = 73.2 \pm 1.3 \text{ kms}^{-1} \text{ Mpc}^{-1}$  (Riess et al. 2021); however, choosing a different value that *combines* various direct measurements would not affect the result, given their small differences.
- The KIDS1000+BOSS+2dfLenS weak lensing data, compressed as a split-normal likelihood on the parameter  $S_8 = 0.766^{+0.02}_{-0.014}$  (Heymans et al. 2021).
- The Gaussian prior on absolute magnitude  $M_B = -19.244 \pm 0.037 \text{ mag}$  (Camarena & Marra 2021), corresponding to the SN measurements from SH0ES.

### 3.2. Methodology

Our baseline cosmology consists in the following combination of the six  $\Lambda$ CDM parameters  $\{\omega_b, \omega_{\text{cdm}}, 100 \times \theta_s, n_s, \ln(10^{10}A_s), \tau_{\text{reio}}\}$ , plus four dark energy equation of state parameters as discussed in Section 2, namely  $w_0, w_m, a_p, \Delta_{\text{de}}$ , and neutrino mass  $\Sigma m_\nu$ . We dub this model as  $\nu$ 4pDE. We run Markov Chain Monte Carlo (MCMC) analysis of the  $\nu$ 4pDE model against various combinations of the CMB, BAO, and supernovae data sets (details of which are given in Section 3.1) with the Metropolis–Hasting algorithm as implemented in the MontePython-v3 (Brinckmann 2019) code interfaced with our modified version of CLASS. We use the prior ranges for the  $\nu$ 4pDE model as given in Table 1; priors for the other six base parameters  $\{\omega_b, \omega_{\text{cdm}}, 100 \times \theta_s, n_s, \ln(10^{10}A_s), \tau_{\text{reio}}\}$  are kept the same as the default set into the MontePython-v3 (Brinckmann 2019) code. All reported  $\chi^2_{\text{min}}$  are obtained with the python package IMINUIT<sup>1</sup> (James & Roos 1975). We make

use of a Choleski decomposition to better handle the large number of nuisance parameters (Lewis et al. 2000) and consider chains to be converged with the Gelman–Rubin convergence criterion  $R-1 < 0.05$  (Gelman & Rubin 1992). We also run MCMC chains for the standard  $\Lambda$ CDM and  $\nu$ CPL (CPL parameterization with neutrino mass as a free parameter) models with different combinations of data sets and priors for making comparisons.

## 4. Results

We ran three sets of models, the first one is the standard “ $\Lambda$ CDM model.” The other two are dynamical dark energy models; namely  $\nu$ 4pDE and  $\nu$ CPL models. Each model is constrained with combinations of the data sets, Planck TT, EE, TE+Planck lensing (see Section 3.1) dubbed as “Planck,” BAO, and Pantheon (see Section 3.1), together dubbed as “Ext” and the priors  $H_0, M_B,$  and  $S_8$  (see Section 3.1) dubbed as “H0,” “MB,” and “S8,” respectively. We use the standard  $\Lambda$ CDM model with the Planck+Ext data set as our base model for computing  $\Delta\chi^2$  values. The values for  $\nu$ 4pDE model corresponding to different data set/prior combinations are reported in Table 2.

The results of the  $\nu$ 4pDE model with combined data sets for various cases are reported in Table 3, the 2D posterior distributions ( $H_0, M_B, S_8,$  and  $\Sigma m_\nu$ ) are shown in Figure 3. The results of the  $\nu$ CPL model with combined data sets for various cases are reported in Table 4, and the 2D posterior distributions are shown in Figure 4. The 1D posterior distributions of the dark energy equation of state parameters for the  $\nu$ 4pDE model are shown in Figure 5.

We find that  $w_0$  is well constrained for each data set combination and is consistent with the cosmological constant. However, the other three DE parameters are less constrained or unconstrained. Especially in the case of parameter  $\log_{10}(a_1)$  we

<sup>1</sup> <https://iminuit.readthedocs.io/>

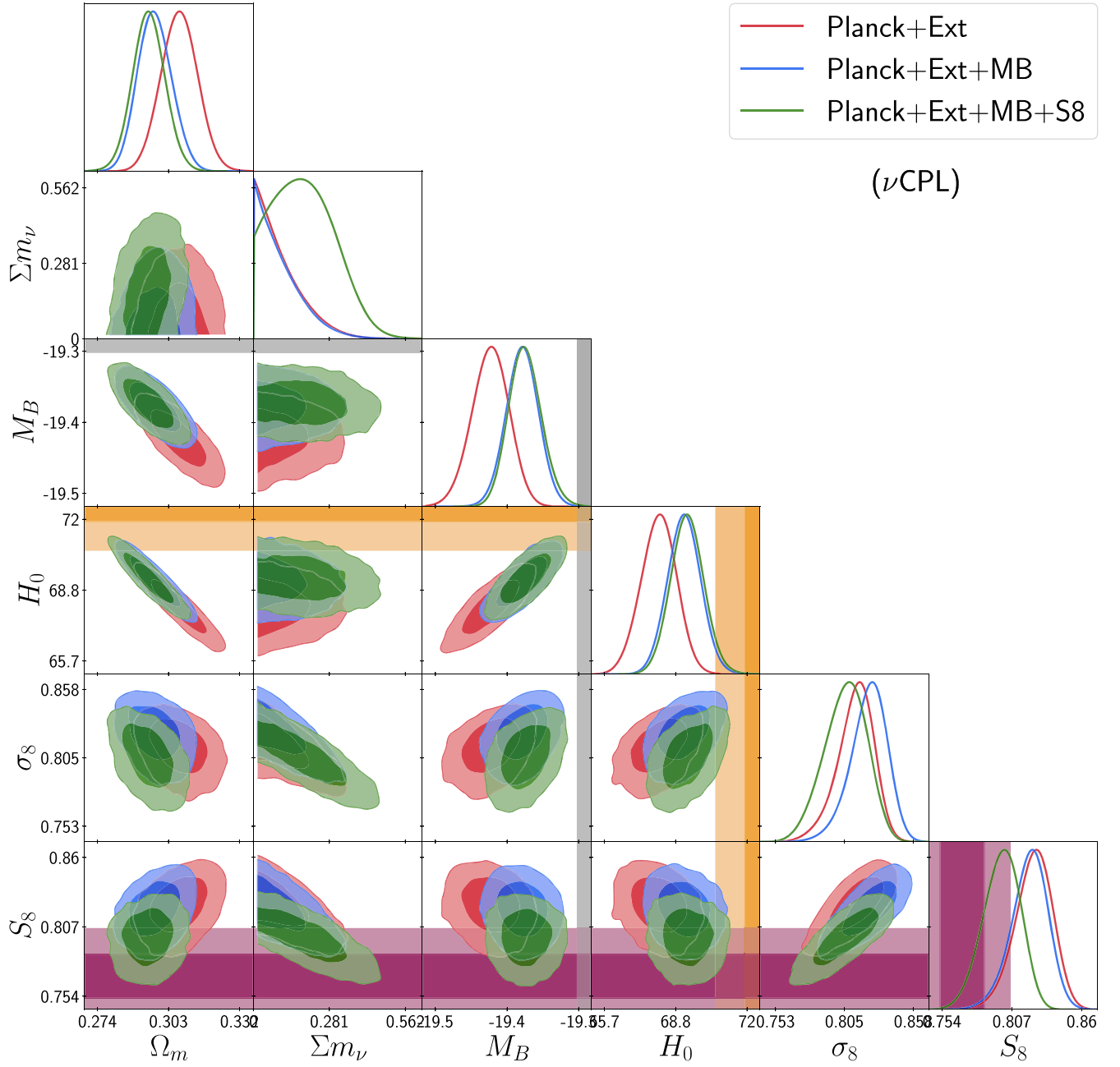


**Figure 4.** 2D posterior distributions of  $(\Omega_m, \Sigma m_\nu, M_B, H_0, \sigma_8, S_8)$  for the  $\nu$ CPL model with Planck+Ext data and a different prior combination. We have also added 68% (dark orange) and 95% (light orange) bands corresponding to a  $H_0$  measurement from SH0ES and 68% (dark purple) and 95% (light purple) bands corresponding to a  $S_8$  measurement from KIDS1000+BOSS+2dfLenS.

do not find the lower bound. This is not surprising given the fact the data does not seem to be favoring very sharp transition, i.e., a very small value for  $\Delta_{de}$ , in that case  $w_{de}(z)$  has a rather weak dependence on the parameter  $a_r$  (see Equations (3) and (4)) and hence resulting in weak constraints on the parameter  $a_r$ . The overall  $\Delta\chi_{\min}^2$  is  $-1.7$  compared to our base  $\Lambda$ CDM model, though we still have the  $H_0$  tension at  $\sim 3.2\sigma$  and  $S_8$  tension at  $\sim 2.5\sigma$  with this model.

When using the  $M_B$  prior, there is no major impact on the equation of state parameters except the values of  $w_m$  shift to slightly more negative. In this case, the model has a  $H_0$  tension at  $\sim 2.6\sigma$  with the SH0ES results. The overall  $\chi_{\min}^2$  shift is  $-6.5$  compared to the  $\Lambda$ CDM model.

For the case when  $M_B$  and  $S_8$  priors are applied simultaneously, we find that  $H_0$  attains a high value, and there is a decrease in the  $S_8$  value, i.e., we find negative correlation between parameter  $S_8$  and  $H_0$  in this case (see Figure 3). This model brings down the  $S_8$  tension below  $\leq 1.5\sigma$  and the  $H_0$  tension from  $\leq 2.5\sigma$ . In this case, we also get a peak in the posterior of the neutrino mass (see Figure 3).

#### 4.1. Comparison between the $\nu$ CPL Model and the $\nu$ 4pDE Model

We also run the  $\nu$ CPL model with the same data combinations. Results of this model are reported in Table 4 and the 2D posterior distributions are shown in Figure 4. Both

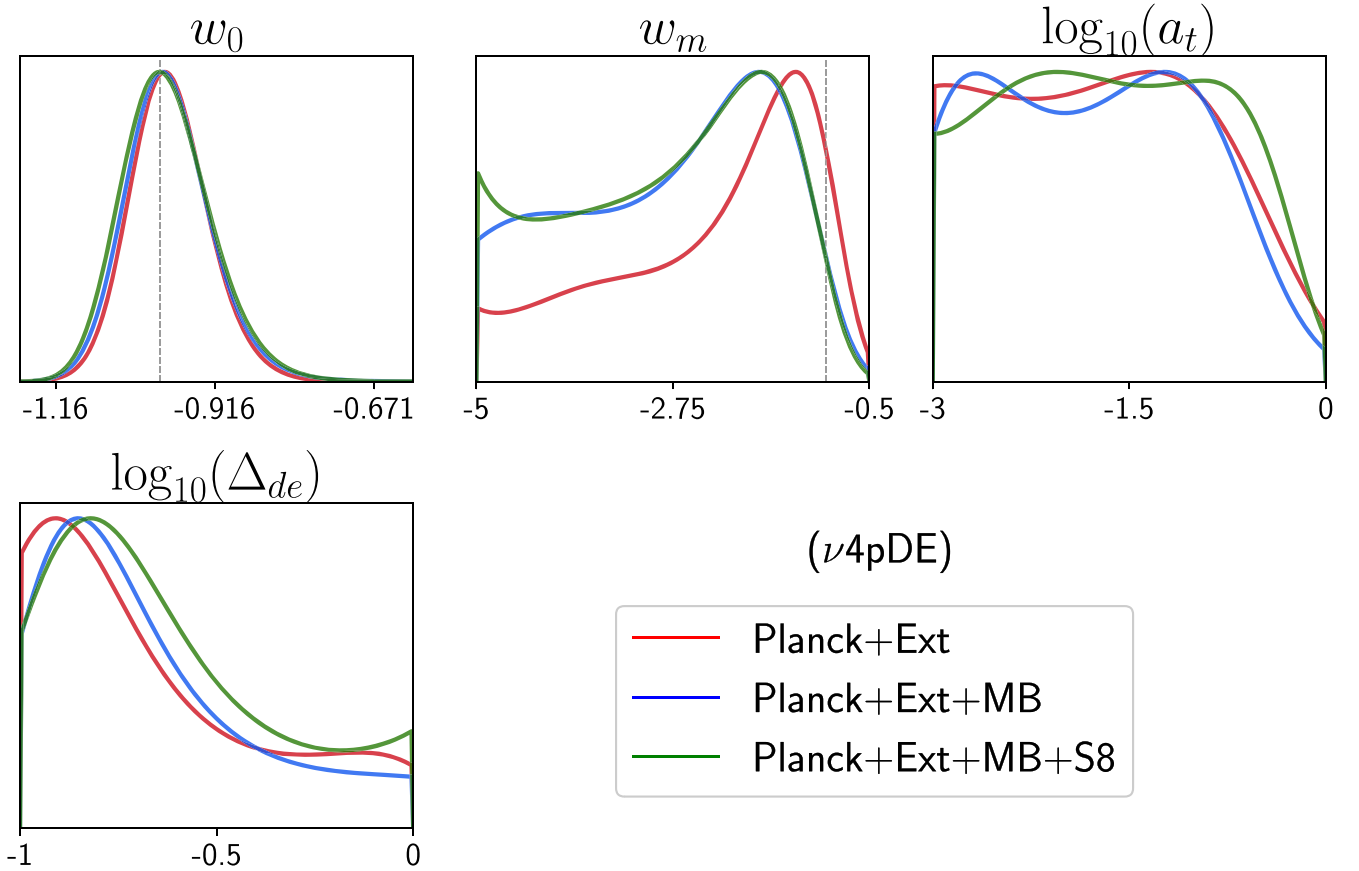


**Figure 5.** 1D posterior distributions of equation of state parameters  $\{w_0, w_m, \log_{10}(a_t), \log_{10}(\Delta_{de})\}$  for the  $\nu 4pde$  model with Planck+Ext data and different prior combinations (see legends).

the parameters  $w_0$  and  $w_a$  are well constrained for the  $\nu CPL$  model. We find the posterior distribution of main cosmological parameters  $\{\omega_b, \omega_{cdm}, 100 \times \theta_s, n_s, \ln(10^{10} A_s), \tau_{reio}\}$  of this model are matched with the  $\nu 4pDE$  model. However the model parameters ( $w_0$  and  $w_a$ ) are different for obvious reasons.

Figure 6 shows a comparison among the  $\nu 4pDE$ ,  $\nu CPL$ , and the base  $\Lambda CDM$  model in terms of the 1D posteriors of parameters  $\{H_0, S_8, w_0, \Sigma m_\nu\}$ . The parameter  $w_0$  is constrained more in the  $\nu 4pDE$  model compared to the  $\nu CPL$  model. However, when we do not use any prior, we do not notice a significant change in  $H_0$  and  $S_8$  compared to the  $\Lambda CDM$  model. But when we use an  $M_B$  prior, the level of  $H_0$  tension is reduced, and is within a  $2.5\sigma$  level with the SH0ES measurement. Similarly, when we add an  $S_8$  prior, we notice a slight reduction in the  $S_8$  parameter also.

#### 4.2. Comparison between the $H_0$ Prior and the $M_B$ Prior

When using the prior on  $H_0$  instead of  $M_B$ , the main impact on results is on the parameters  $w_0$  and  $H_0$ . The parameter  $H_0$  attains a slightly higher value compared to the  $M_B$  prior case and  $w_0$  shifts toward a lower value. The results are compared in Figure 6. This result is true for the  $\nu CPL$  model as well. We also see that the  $H_0$  prior supports a nonzero neutrino mass more in comparison to the  $M_B$  prior. In summary we say that use of the  $H_0$  prior has a stronger impact on the  $w_0, \Sigma m_\nu$ , and for obvious reasons on  $H_0$  compared to the case with the  $M_B$  prior.

## 5. Conclusions and Discussion

We have investigated a generic model of nonlinearly evolving dynamical dark energy equation of state  $w$  with massive neutrinos (the  $\nu 4pDE$  model), in light of the recent Planck, Pantheon, and BAO data, and recent measurements of  $H_0$  and  $S_8$ . We have studied the effect of such parameterization on the background and derived cosmological parameters. The results of our analysis are in accordance with the earlier studies with a linear evolution of  $w_{de}$  (CPL-like; Di Valentino et al. 2015, 2016b, 2017; Poulin et al. 2018) and a few other parameterizations of dynamical dark energy (Zhang et al. 2017; Zhao et al. 2017; Bhattacharyya et al. 2019). We do not get any strong constraints on the two extra parameters  $a_t$  and  $\Delta_{de}$  at  $\gtrsim 1\sigma$  level; constraints on  $w_0$  are in good agreement with the  $\nu CPL$  parameterization. However, we do get slightly different and a more tightly constrained  $w_0$  when the model is tested against Planck and external data (Pantheon+BAO) put together. The added external prior on parameters  $M_B$  and  $S_8$  makes the difference in  $\nu CPL$  and  $\nu 4pDE$  parameterization even broader. The  $\nu 4pDE$  model can bring down the Hubble tension to  $\sim 2.5\sigma$  level and the  $S_8$  tension to  $\sim 1.5\sigma$  level when tested against Planck, BAO, and Pantheon supernovae data together. More importantly, we find that there is a slightly negative correlation between the parameters  $S_8$  and  $H_0$  with the  $\nu 4pDE$  model, which is very interesting.

However, both the  $\nu 4pDE$  model and  $\nu CPL$  model improve  $\Delta\chi_{min}^2$  for the Planck+Ext data set and the recent measurements of  $H_0$  and  $S_8$  in comparison to  $\Lambda CDM$ ; this lowering of  $\chi_{min}^2$  is achieved at the expense of adding extra parameters. So



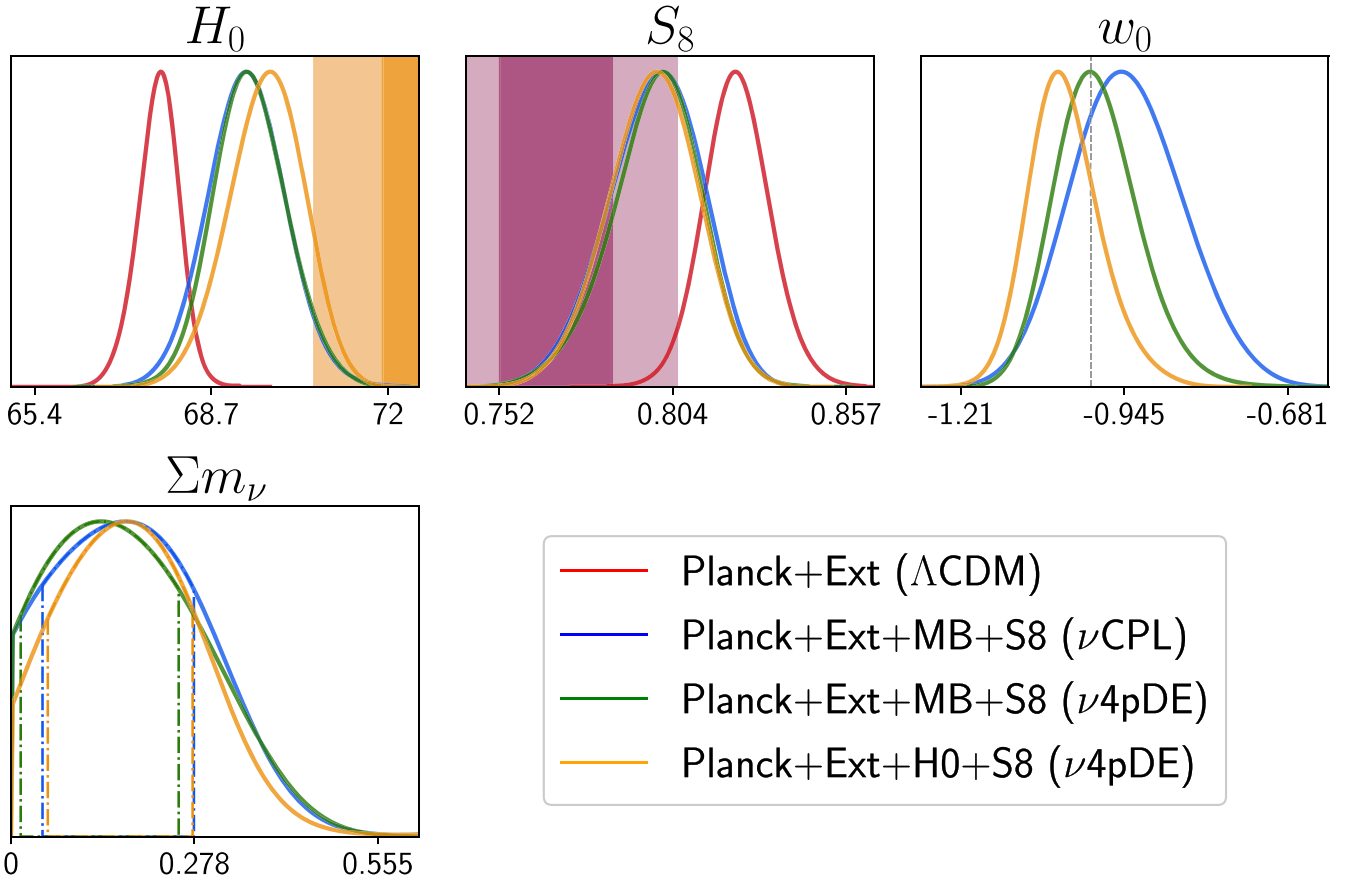


**Figure 6.** 1D posterior distributions of ( $H_0$ ,  $S_8$ ,  $w_0$ ,  $\Sigma m_\nu$ ) for different models and combinations of priors (see legends). The dotted–dashed vertical lines in the  $\Sigma m_\nu$  panel correspond to respective  $1\sigma$  levels.

**Table 5**

Comparison of  $\Delta\chi^2_{\min}$  and  $\Delta\text{AIC}$  for the  $\nu 4\text{pDE}$  and  $\nu\text{CPL}$  Models

Data → Model ↓	Planck+Ext+MB		Planck+Ext+MB+S8	
	$\Delta\chi^2_{\min}$	$\Delta\text{AIC}$	$\Delta\chi^2_{\min}$	$\Delta\text{AIC}$
$\Lambda\text{CDM}$	0	0	0	0
$\nu\text{CPL}$	-7.23	-1.23	-2.76	+3.24
$\nu 4\text{pDE}$	-6.53	+3.47	-5.50	+4.50

if we follow  $\Delta\text{AIC}$  criteria<sup>2</sup>, the level of success of these models degrades as none of the models have significantly improved the  $\Delta\text{AIC}$  value over the  $\Lambda\text{CDM}$  model. From Table 5 it is evident that when considered Planck+Ext+MB,  $\nu\text{CPL}$  is still a preferred model. But when we consider Planck+Ext+MB+S8, all the models ( $4\text{pDE}$ ,  $\nu 4\text{pDE}$ ,  $\nu\text{CPL}$ ) perform worse in comparison to  $\Lambda\text{CDM}$ .

We also see that with an added  $S_8$  prior  $\nu 4\text{pDE}$  favors a nonzero value for the neutrino mass parameter ( $\Sigma m_\nu \sim 0.2 \pm 0.1$  eV), which is in agreement with earlier work using the  $\nu\text{CPL}$  parameterization (Poulin et al. 2018); however our

analysis does not detect a lower bound on the  $\Sigma m_\nu$  parameter at  $\gtrsim 1\sigma$ . Earlier work such as Poulin et al. (2018) where 2015 Planck data have been used, the neutrino mass  $\Sigma m_\nu$  was found to be nonzero even at  $\gtrsim 2\sigma$ . Also in a recent work Di Valentino & Melchiorri (2022) report a nonzero value for the neutrino mass when using WMAP data along with ACT-DR4, and SPT-3G data. However they also get similar results on  $\Sigma m_\nu$  as ours when recent Planck and BAO data are used. The well-known lensing anomaly in the Planck data ( $A_{\text{lens}} \neq 1$ ) could be playing a role here, which needs to be investigated further in more detail.

We thank Vivian Poulin for reading the draft and for his valuable inputs. We thank Pier Stefano Corasaniti, Eoin O Colgain, and Sunny Vagnozzi for their valuable inputs. S.D. and K.P. acknowledge SERB DST Government of India grant CRG/2019/006147 for supporting the project. We acknowledge HPC NOVA, IIA Bangalore where numerical simulations were performed.

## Appendix

### Effect of Varying 4pDE Equation of State Parameters on BAO and Supernovae Observables

The dark energy equation of state parameter  $w_0$  is most sensitive to observables because it is the equation of state when the dark energy density is dominating the universe. So an increase in the value of this parameter rapidly increases the dark energy density and the expansion rate of the

<sup>2</sup> Akaike Information Criterion (AIC) is one of the popular methods of estimating the relative quality of proposed models for given data. AIC is based on using a trade off between the goodness of fit of the model and the simplicity. AIC uses model's log likelihood as a measure of fit and the number of parameters in the model as the complexity of the model. If  $N_{\text{Model}}$  is the total number of parameters in a model the AIC score for that model is given by

$$\Delta\text{AIC} = \chi^2_{\min, \text{Model}} - \chi^2_{\min, \Lambda\text{CDM}} + 2(N_{\text{Model}} - N_{\Lambda\text{CDM}}).$$

universe hence having a major impact on the late-time observables. This fact is evident from the upper left panels of Figures 7, 8, and 9. The  $w_m$  parameter is the DE equation of state at earlier times. At that time the amount of dark energy density was relatively less. So this equation of state parameter has less impact on the observables. The upper right panels of Figures 7, 8, and 9 show the impact of varying  $w_m$  on various observables. We can see that the change in the observables are relatively low in comparison to

the case of parameter  $w_0$ . The DE parameters  $a_t$  and  $\Delta_{de}$  determine the width and the epoch of transition of the equation of state from  $w_m$  to  $w_0$ . The effects of varying  $a_t$  and  $\Delta_{de}$  are shown in the down-left and the down-right panels of Figures 7, 8, and 9, respectively. We can see that parameter  $a_t$  has the least impact on the observables given the smooth (large width) transition preferred by the data. We also see that the DE parameter  $\Delta_{de}$  has comparatively more impact on the observables.

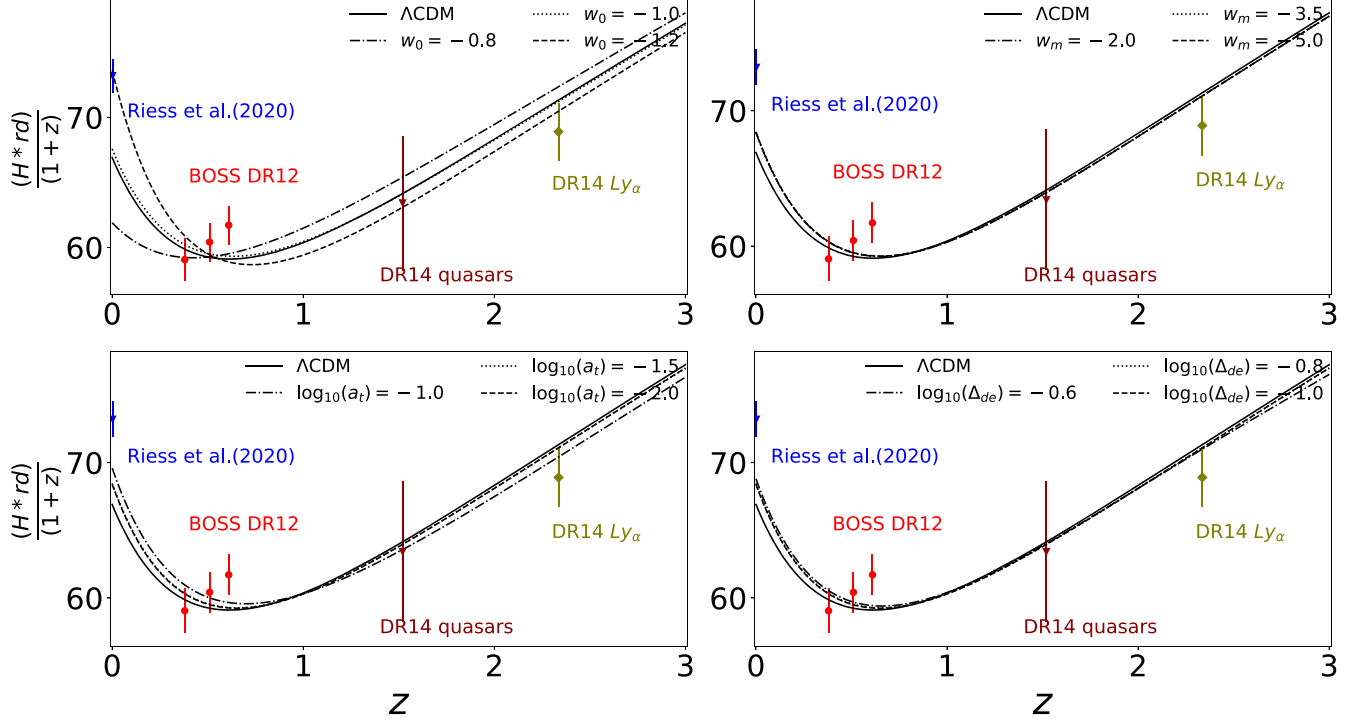


**Figure 7.** The plots of the evolution of  $H(z)r_d/(1+z)$  for 4pDE models and the reference  $\Lambda$ CDM model. Each of the four panels show effects of varying different dark energy equation of state parameters (see the legends) while fixing other EOS parameters to values ( $w_0 = -1.03$ ,  $w_m = -3.97$ ,  $\log_{10}(a_t) = -1.63$ ,  $\log_{10}(\Delta_{de}) = -0.87$ ).

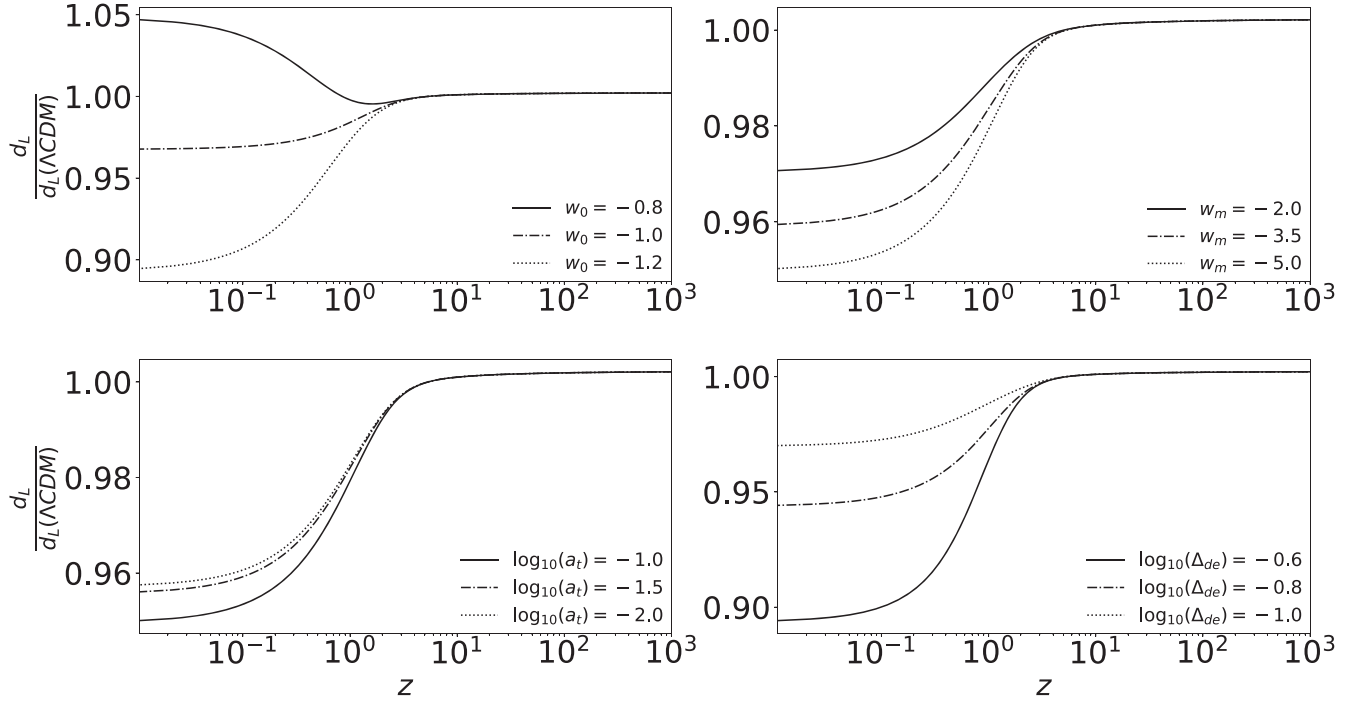


**Figure 9.** The plots of the evolution of the luminosity distance as a function of redshift for the 4pDE model and  $\Lambda\text{CDM}$  model. Each of the four panels show effects of varying different dark energy equation of state parameters (see the legends) while fixing other EOS parameters to values  $(w_0 = -1.03, w_m = -3.97, \log_{10}(a_t) = -1.63, \log_{10}(\Delta_{de}) = -0.87)$ .

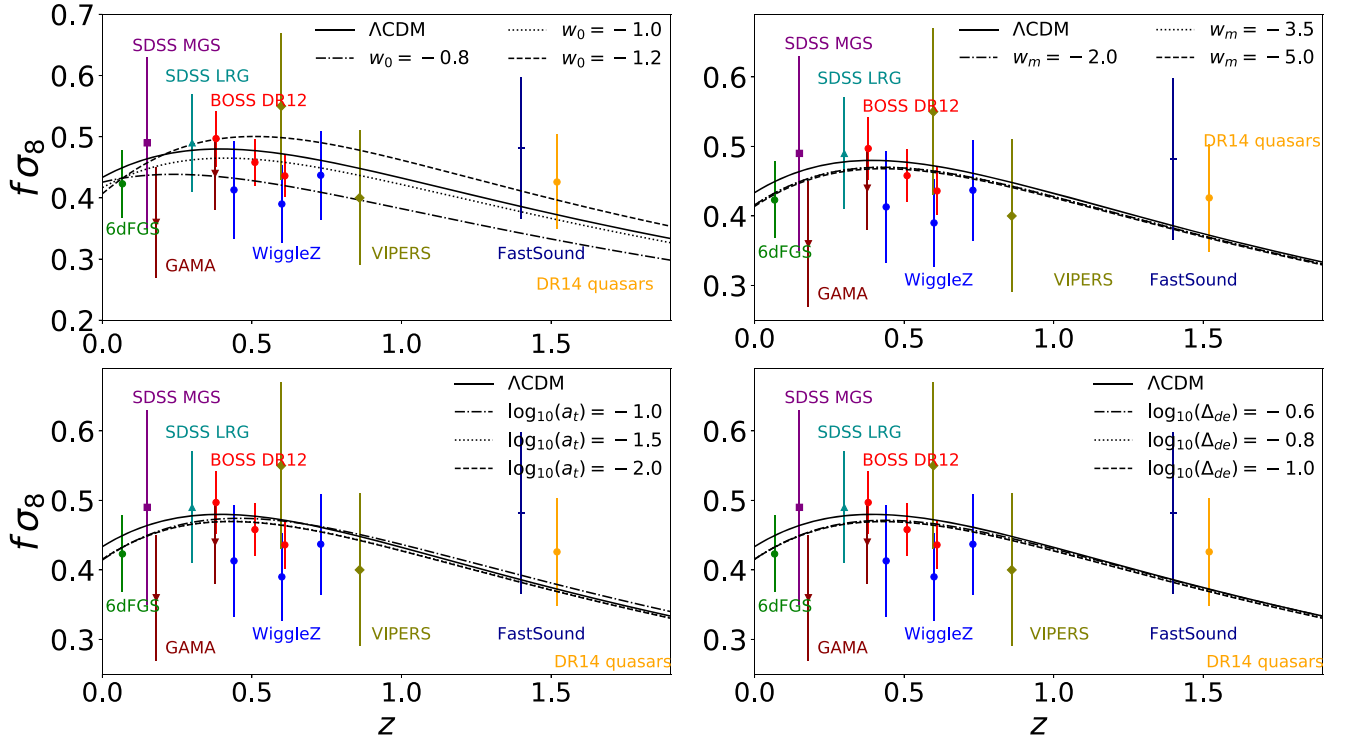


**Figure 8.** The plots of the evolution of the parameter  $f\sigma_8$  as a function of redshift for the 4pDE model and  $\Lambda\text{CDM}$  model. Each of the four panels show effects of varying different dark energy equation of state parameters (see the legends) while fixing other EOS parameters to values  $(w_0 = -1.03, w_m = -3.97, \log_{10}(a_t) = -1.63, \log_{10}(\Delta_{de}) = -0.87)$ .

## ORCID iDs

Kanhaiya Lal Pandey  <https://orcid.org/0000-0003-3536-1730>

Subinoy Das  <https://orcid.org/0000-0002-7771-180X>

## References

- Abbott, T. M. C., Abdalla, F. B., Alarcon, A., et al. 2018, *PhRvD*, **98**, 043526
- Abellán, G. F., Chacko, Z., Dev, A., et al. 2021a, arXiv:2112.13862
- Abellán, G. F., Murgia, R., & Poulin, V. 2021b, *PhRvD*, **104**, 123533
- Alam, S., Ata, M., Bailey, S., et al. 2017, *MNRAS*, **470**, 2617
- Anchordoqui, L. A., Di Valentino, E., Pan, S., & Yang, W. 2021, *JHEAp*, **32**, 28
- Ballardini, M., Finelli, F., Umiltà, C., & Paoletti, D. 2016, *JCAP*, **5**, 067
- Bamba, K., Capozziello, S., Nojiri, S., & Odintsov, S. D. 2012, *Ap&SS*, **342**, 155
- Banerjee, A., Cai, H., Heisenberg, L., et al. 2021, *PhRvD*, **103**, L081305
- Barboza, E. M., Jr., & Alcaniz, J. S. 2008, *PhLB*, **666**, 415
- Benevento, G., Hu, W., & Raveri, M. 2020, *PhRvD*, **101**, 103517
- Beutler, F., Blake, C., Colless, M., et al. 2011, *MNRAS*, **416**, 3017
- Bhattacharyya, A., Alam, U., Lal Pandey, K., Das, S., & Pal, S. 2019, *ApJ*, **876**, 143
- Blomqvist, M., du Mas des Bourboux, H., Busca, N. G., et al. 2019, *A&A*, **629**, A86
- Braglia, M., Ballardini, M., Finelli, F., & Koyama, K. 2021, *PhRvD*, **103**, 043528
- Brinckmann, T., & Lesgourgues, J. 2019, *PDU*, **24**, 100260
- Calabrese, E., Huterer, D., Linder, E. V., Melchiorri, A., & Pagano, L. 2011, *PhRvD*, **83**, 123504
- Camarena, D., & Marra, V. 2021, *MNRAS*, **504**, 5164
- Chevallier, M., & Polarski, D. 2001, *IJMPD*, **10**, 213
- Corasaniti, P. S., & Copeland, E. J. 2003, *PhRvD*, **67**, 063521
- Das, S., Corasaniti, P. S., & Khoury, J. 2006, *PhRvD*, **73**, 083509
- Das, S., Maharana, A., Poulin, V., & Kumar, R. 2022, *PhRvD*, **105**, 103503
- de Sainte Agathe, V., Balland, C., du Mas des Bourboux, H., et al. 2019, *A&A*, **629**, A85
- Di Valentino, E. 2021, *MNRAS*, **502**, 2065
- Di Valentino, E., Giusarma, E., Mena, O., Melchiorri, A., & Silk, J. 2016a, *PhRvD*, **93**, 083527
- Di Valentino, E., & Melchiorri, A. 2022, *ApJL*, **931**, L18
- Di Valentino, E., Melchiorri, A., Linder, E. V., & Silk, J. 2017, *PhRvD*, **96**, 023523
- Di Valentino, E., Melchiorri, A., & Silk, J. 2015, *PhRvD*, **92**, 121302
- Di Valentino, E., Melchiorri, A., & Silk, J. 2016b, *PhLB*, **761**, 242
- Di Valentino, E., Mena, O., Pan, S., et al. 2021a, *CQGra*, **38**, 153001
- Di Valentino, E., Anchordoqui, L. A., Akarsu, Ö, et al. 2021b, *Aph*, **131**, 102605
- Durrive, J.-B., Ooba, J., Ichiki, K., & Sugiyama, N. 2018, *PhRvD*, **97**, 043503
- Efstathiou, G. 1999, *MNRAS*, **310**, 842
- Efstathiou, G. 2021, *MNRAS*, **505**, 3866
- Farhang, M., & Khosravi, N. 2021, *PhRvD*, **103**, 083523
- Freedman, W. L. 2017, *NatAs*, **1**, 0121
- Gelman, A., & Rubin, D. B. 1992, *StaSc*, **7**, 457
- Gogoi, A., Sharma, R. K., Chanda, P., & Das, S. 2021, *ApJ*, **915**, 132
- Hannestad, S. 2005, *PhRvL*, **95**, 221301
- Hazra, D. K., Antony, A., & Shafieloo, A. 2022, arXiv:2201.12000
- Heisenberg, L., Villarrubia-Rojo, H., & Zosso, J. 2022a, arXiv:2202.01202
- Heisenberg, L., Villarrubia-Rojo, H., & Zosso, J. 2022b, arXiv:2201.11623
- Heymans, C., Grocutt, E., Heavens, A., et al. 2013, *MNRAS*, **438**, L1
- Heymans, C., Tröster, T., Asgari, M., et al. 2021, *A&A*, **646**, A140
- Hildebrandt, H., Köhlinger, F., van den Busch, J. L., et al. 2020, *A&A*, **633**, A69
- Jaber, M., & de la Macorra, A. 2018, *Aph*, **97**, 130
- James, F., & Roos, M. 1975, *CoPhC*, **10**, 343
- Jassal, H. K., Bagla, J. S., & Padmanabhan, T. 2005, *PhRvD*, **72**, 103503
- Jassal, H. K., Bagla, J. S., & Padmanabhan, T. 2010, *MNRAS*, **405**, 2639
- Joudaki, S., Hildebrandt, H., Traykova, D., et al. 2020, *A&A*, **638**, L1
- Lemos, P., Lee, E., Efstathiou, G., & Gratton, S. 2019, *MNRAS*, **483**, 4803
- Lewis, A., Challinor, A., & Lasenby, A. 2000, *ApJ*, **538**, 473
- Li, X., & Shafieloo, A. 2019, *ApJL*, **883**, L3
- Linder, E. V. 2003, *PhRvL*, **90**, 091301
- Lorenz, C. S., Calabrese, E., & Alonso, D. 2017, *PhRvD*, **96**, 043510
- MacCrann, N., Zuntz, J., Bridle, S., Jain, B., & Becker, M. R. 2015, *MNRAS*, **451**, 2877
- Marcondes, R. J. F., & Pan, S. 2017, arXiv:1711.06157
- Martins, C. J. A. P., & Colomer, M. P. 2018, *A&A*, **616**, A32
- Mawas, E., Street, L., Gass, R., & Wijewardhana, L. C. R. 2021, arXiv:2108.13317
- Nojiri, S., Odintsov, S. D., & Oikonomou, V. K. 2017, *PhR*, **692**, 1
- Nunes, R. C., & Vagnozzi, S. 2021, *MNRAS*, **505**, 5427
- Ó Colgáin, E., Sheikh-Jabbari, M. M., & Yin, L. 2021, *PhRvD*, **104**, 023510
- Pandey, K. L., Karwal, T., & Das, S. 2020, *JCAP*, **2020**, 026
- Planck Collaboration, Aghanim, N., Akrami, Y., et al. 2020, *A&A*, **641**, A6
- Poulin, V., Boddy, K. K., Bird, S., & Kamionkowski, M. 2018, *PhRvD*, **97**, 123504
- Poulin, V., Serpico, P. D., & Lesgourgues, J. 2016, *JCAP*, **08**, 036
- Poulin, V., Smith, T. L., Karwal, T., & Kamionkowski, M. 2019, *PhRvL*, **122**, 221301
- Riess, A. G., Casertano, S., Yuan, W., et al. 2021, *ApJL*, **908**, L6
- Riess, A. G., Casertano, S., Yuan, W., Macri, L. M., & Scolnic, D. 2019, *ApJ*, **876**, 85
- Ross, A. J., Samushia, L., Howlett, C., et al. 2015, *MNRAS*, **449**, 835
- Roy, N., Goswami, S., & Das, S. 2022, *PDU*, **36**, 101037
- Sahni, V. 2002, *CQGra*, **19**, 3435
- Schöneberg, N., Franco Abellán, G., Pérez Sánchez, A., et al. 2021, arXiv:2107.10291
- Scolnic, D. M., Jones, D. O., Rest, A., et al. 2018, *ApJ*, **859**, 101
- Sutherland, W. 2018, *MNRAS*, **477**, 1913
- Theodoropoulos, A., & Perivolaropoulos, L. 2021, *Univ*, **7**, 300
- Vagnozzi, S. 2020, *PhRvD*, **102**, 023518
- Vagnozzi, S., Dhawan, S., Gerbino, M., et al. 2018, *PhRvD*, **98**, 083501
- Vagnozzi, S., Giusarma, E., Mena, O., et al. 2017, *PhRvD*, **96**, 123503
- Visinelli, L., Vagnozzi, S., & Danielsson, U. 2019, *Symm*, **11**, 1035
- Yang, W., Di Valentino, E., Pan, S., Shafieloo, A., & Li, X. 2021a, *PhRvD*, **104**, 063521
- Yang, W., Di Valentino, E., Pan, S., Wu, Y., & Lu, J. 2021b, *MNRAS*, **501**, 5845
- Zhang, Y.-C., Zhang, H.-Y., Wang, D.-D., et al. 2017, *RAA*, **17**, 050
- Zhao, G.-B., Raveri, M., Pogosian, L., et al. 2017, *NatAs*, **1**, 627